J. Plasma Physics (2009), *vol.* 75, *part* 6, *pp.* 787–798. © Cambridge University Press 2009
doi:10.1017/S0022377809007909

Effects of diode current on high power microwave generation in a vircator

GUOZHI LIU, WENHUA HUANG, HAO SHAO, SHI QIU, HONGJUN WANG, JINGYUE LIU, FENG WANG, ZHANFENG YANG and YONGZHI QIAO

(shaohaonint@163.com)

(Received 29 December 2008 and accepted 7 January 2009, first published online 15 April 2009)

Abstract. An experiment of a virtual cathode oscillator (vircator) built on the low impedance intense electron beam accelerator Flash II is reported. A novel spectrum diagnosis method—a circulating dispersion line—is proposed. A thin oil layer coated graphite cathode is introduced in the experiment to decrease the delay time of the explosive emission process and obtain a homogeneous electron beam emission for improving the high-power microwave (HPM) generation efficiency. The effect of diode current on HPM generation in the vircator system is discussed. The HPM pulse width has a strong connection with the diode current waveform. For most shots, corresponding to the time that microwave emission starts, there is an inflection point in the diode current pulse. Compared with the case that no microwave is generated, the diode current increases more slowly following the inflection point. HPM generation terminates when the beam current reaches the self-pinching critical current of the diode.

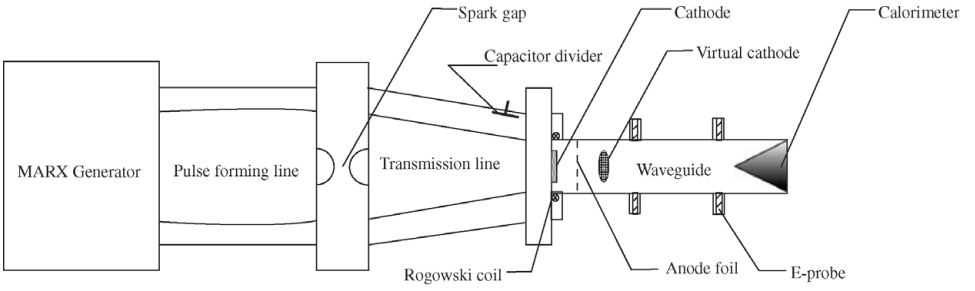
1. Introduction

Over the past few decades, high-power microwave (HPM) research has continued on the virtual cathode oscillator (vircator) with varied results [1–4]. The vircator has remained of interest primarily because the device geometry is relatively simple and hence easy to build. Additionally, unlike most other HPM devices, the vircator requires no external magnetic field. The vircator is also one of the most promising high-power microwave sources due to its output power capability and tuneability over several octaves.

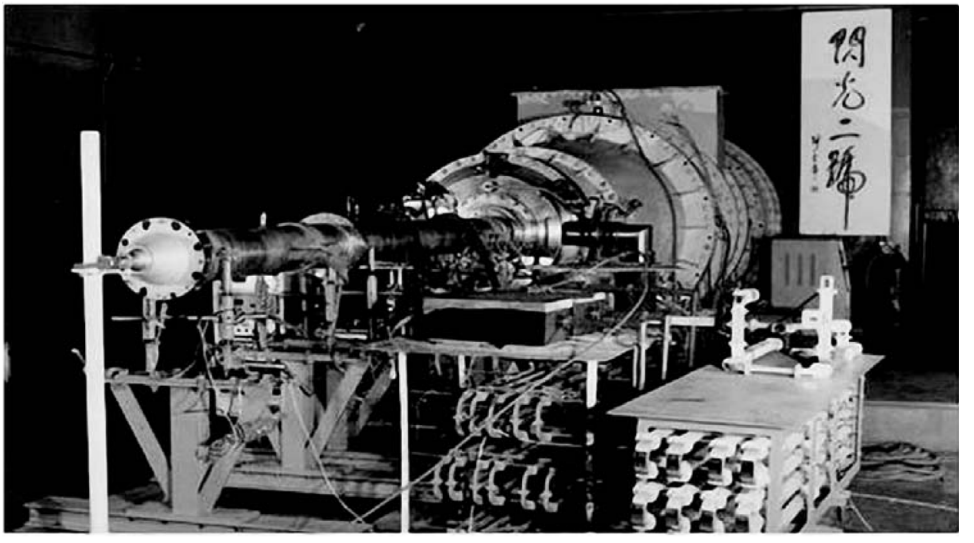
After nearly 15 years of dumbness, vircators are now enjoying something of a renaissance and developments with novel configurations are proposed to overcome two problems that plagued devices of this type: low efficiency and sensitivity to gap closure in the high current. However, further researches are still required on the microwave generation mechanism and the factors which affect the performance of the vircator.

Parts of the experimental results obtained from the vircator system conducted on the low impedance intense electron beam accelerator Flash II are analyzed and discussed. The diode current effects on HPM generation in the vircator are given emphasis in the discussion as well as the experimental system design.

https://doi.org/10.1017/S0022377809007909 Published online by Cambridge University Press



(a)



(b)

Figure 1. Schematic diagram and experimental configuration of vircator on Flash-II. (a) Schematic diagram of Flash-II vircator. (b) Experimental configuration of Flash-II vircator.

2. Experimental setup and parameter diagnosis

The schematic diagram of the experimental setup is shown in Fig. 1. The vircator is driven by a 0.8 MeV, 400 kA, and 80 ns high-power electron beam generator, Flash-II. The electron beam is emitted from graphite cathodes with diameters of 18 cm or 22 cm and penetrates through the grounded 12 μm thick aluminized-mylar anode foil (1.0 μm thick aluminum and 11 μm thick mylar). A virtual cathode forms inside the overmoded circulating waveguide, which is a stainless steel cylinder of 29.2 cm inner diameter and 206 cm length. The typical operation pressure inside the waveguide and diode is kept in the range of 10^{-2} Pa to 10^{-3} Pa.

Experimental diagnosis systems are composed of the beam and microwave parameter measurements. The beam diagnosis system includes a B-dot probe, a self-integrating Rogowski coil embedded in the anode cylinder, and a capacitive divider. The beam current of the diode is given by the Rogowski coil, and the B-dot probe measures the time differential of the total diode current, di_D/dt. The electron beam voltage is obtained as $L_D \cdot (di_D/dt)$, from the voltage waveform on the transmission

https://doi.org/10.1017/S0022377809007909 Published online by Cambridge University Press

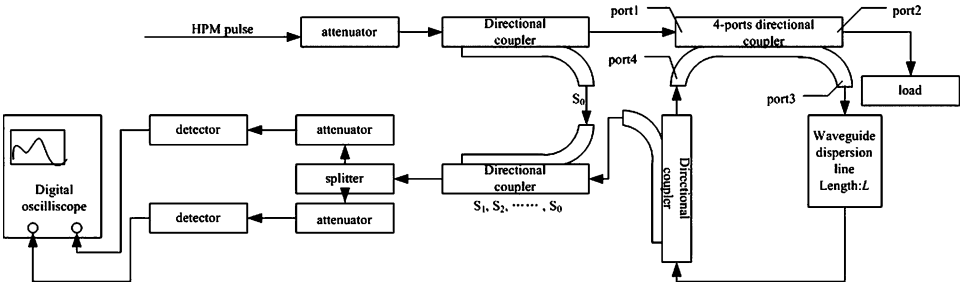


Figure 2. Schematic diagram of the circulating dispersion line.

line, V_{D2}, measured by the capacitive divider, i.e. the diode voltage is determined by the equation

$$V_D = V_{D2} - L_D \cdot (di_D/dt), \tag{1}$$

where L_D is the inductance of the diode, which can be determined by a short-circuit experiment.

The output microwave is axially extracted in the experimental system (shown in Fig. 1(a)). A microwave calorimeter is located at the end of the 2.06 m long waveguide to measure the HPM pulse energy as well as decrease the end reflection. Several E-probes are employed for microwave frequency and power measurements. The coupled signals from the E-probes are transmitted through a directional coupler and attenuators to a crystal detector or circulating dispersion line, allowing power and frequency measurements in X-band and S-band.

Generally, the spectrum of the microwave generated by the vircator is complex. For determining the frequency components of the HPM pulse generated by the vircator system, a circulating dispersion line was firstly proposed and applied in the experiment by the research group in Northwest Institute of Nuclear Technology in 1999 [5]. Generally, for complicated frequency detection, a sufficiently long dispersion line should be used to separate the different frequency components with different transmitted delay times. Hence, for separating the different frequencies in several tens of nanoseconds, over 100 m or even longer of dispersion waveguide should be used. But, in the circulating dispersion line system, the length of the waveguide is reduced to 1/4 to 1/6 of the former one.

The microwave pulse is transmitted inside the closed ring several times for different frequency components and then they could be distinguished by their delay times. If the pulse that has been transmitted n times in the circulating dispersion line can be detected, then the equivalent transmission distance is $L_n = n \cdot L, n$ times the actual length L, and the frequency resolution is n times higher than that of a normal waveguide dispersion line with the same length. Meanwhile, the circulating dispersion line is capable of measuring the time-dependence relation for microwave frequency components. Figure 2 shows a schematic diagram of the circulating dispersion line.

With a low insertion loss, the 6th circular pulse can be detected by a single detector. In the experiment, the WR90 circulating dispersion line is used to detect the frequency component in the range of 8–12 GHz with an approximate length of 19 m. The WR159 circulating dispersion line is used for the frequency range of 4.9–7 GHz with the length of 8 m. By this means, the frequency diagnosis system gives the detection results with a deviation within 2%.

https://doi.org/10.1017/S0022377809007909 Published online by Cambridge University Press

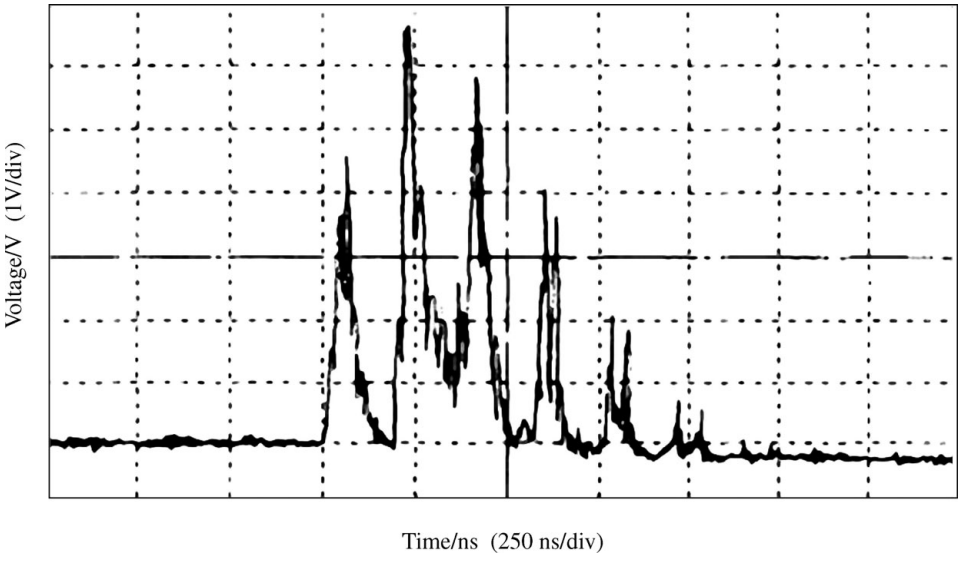


Figure 3. Typical waveform measured by WR159 circulating dispersive line.

3. Experimental results and discussion

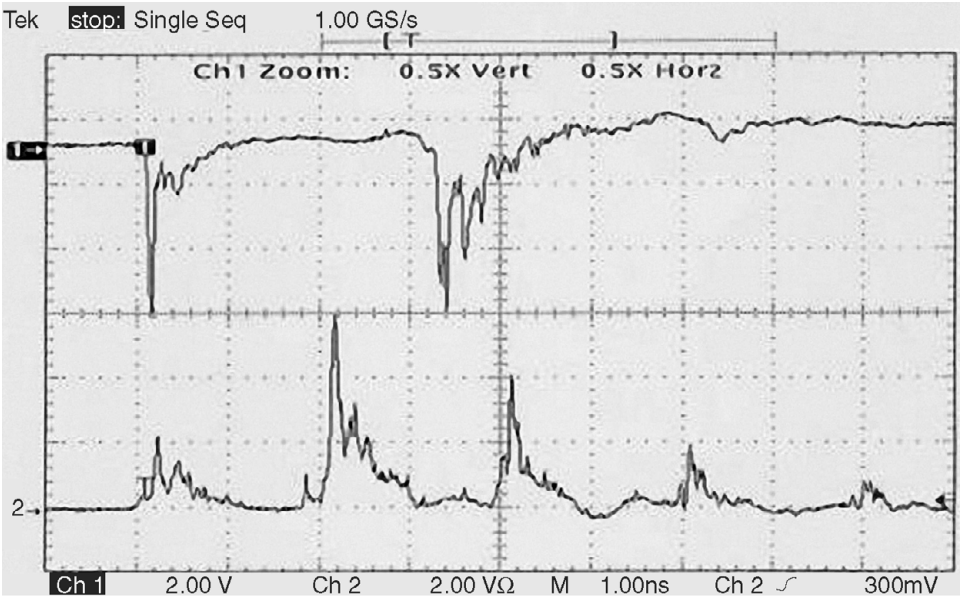
The vircator system is operated under about 300 kA diode current and 1-MV diode voltage. The graphite cathodes with 18 cm or 22 cm diameters are employed in the experimental system. We believe that most of initial explosive points on the field-induced explosive emission cathode are impurities on the cathode surface, and the initial plasma mainly originates from the desorbed gases and ionization of impurities and oxides on the metallic surface [6, 7]. Accordingly, for decreasing the delay time of the explosive emission process and obtaining a homogeneous electron beam emission, the graphite cathodes are coated with a thin transformer oil layer. The explosive emission delay is evidently decreased as well as a uniform emission on the cathode surface being observed. The detailing description is given in [8].

The measured microwave power obtained by combining calorimeter and E-probe ranges from GWs to tens of GW. For preventing the electron beam and anode mesh fragments bombarding the calorimeter, which will lead to a large error of the energy measurement, a polytetrafluoroethylene plate is placed between the diode and the calorimeter. Since the beam–wave interaction cavity and output waveguide are overmoded, the generated HPM will tend to be composed of hybrid modes under rather unconfined stimulation. In the following, we will focus mainly on the diode current effects on the HPM generation from the vircator.

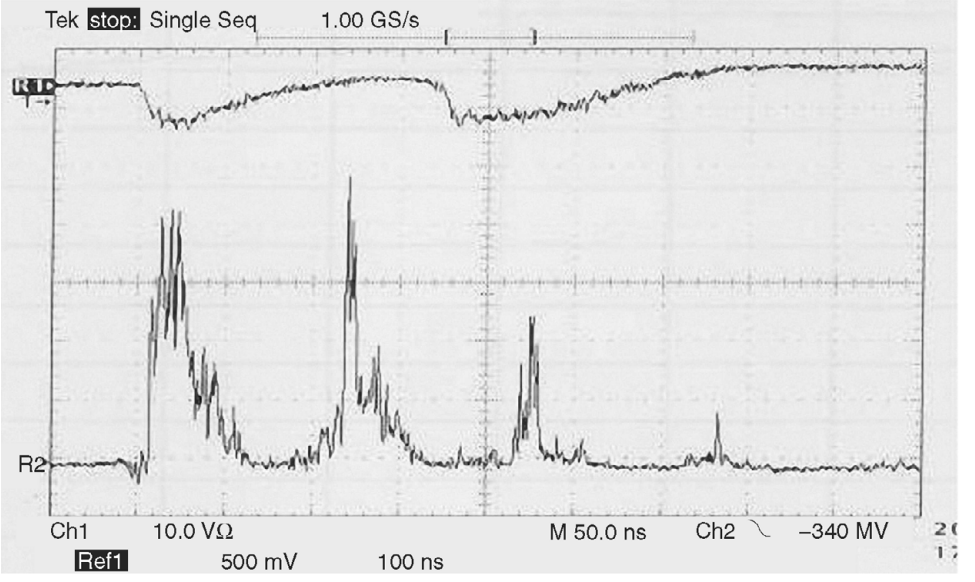
3.1. Frequency diagnosis

The HPM spectrum of most vircators comprises several or even tens of frequency protrusions, especially for the case with a high current. Figure 3 gives the typical HPM pulse waveforms after dispersion cycles measured by a WR159 circulating dispersion line, which apparently shows two main frequencies. Figure 4(a) gives the waveforms separately measured by WR159 and WR90 circulating dispersion lines. The results show that the generated HPM ranges from S-band to X-band when the A–K gap is less than a certain value. But, for most cases, there are no obvious

https://doi.org/10.1017/S0022377809007909 Published online by Cambridge University Press



(a)



(b)

Figure 4. HPM pulse waveforms obtained from WR159 (a) and WR90 (b) circulating dispersion lines.

X-band components detected, as shown in Fig. 4(b). The microwave power is relatively higher when the dominant frequency is notable. The frequency shift corresponds to the fluctuation of the diode current, which is caused by the cathode plasma motion that finally affects the actual A–K gap. The comparison between dominant frequencies given by the circulating dispersion line with A–K gaps of

https://doi.org/10.1017/S0022377809007909 Published online by Cambridge University Press

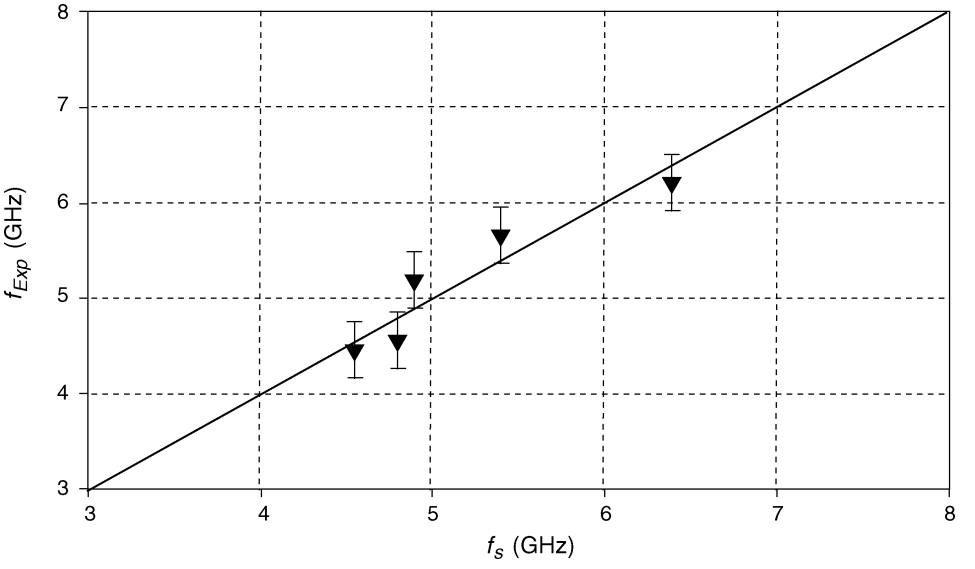


Figure 5. Comparison between the measured frequency and the frequency calculated from (2).

1.3 cm, 1.5 cm, 1.6 cm, 1.8 cm, and 2.0 cm, respectively, and the frequencies calculated from (2), are given in Fig. 5 [9], which illustrates a good agreement in the frequency range studied. It should also be noted that, firstly, the measured frequency is not single, but a narrow span, and sometimes there is no dominant frequency; secondly, dispersion still exists in the dominant frequency, i.e. the main frequency changes even under other parameters and operation terms staying relatively stable.

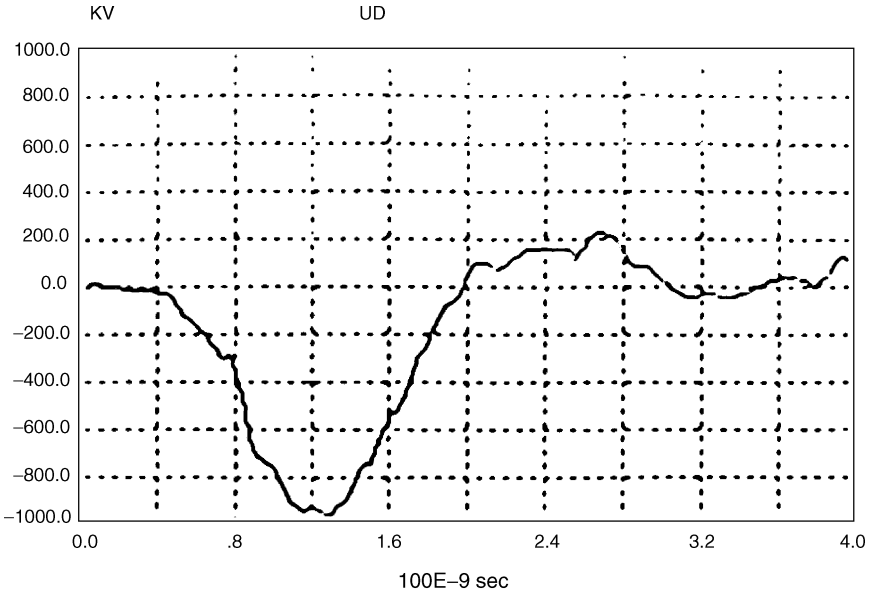
$$f = \frac{4.77}{d} \ln(\gamma + \sqrt{\gamma^2 - 1}). \tag{2}$$

3.2. Correlation between HPM generation and diode current

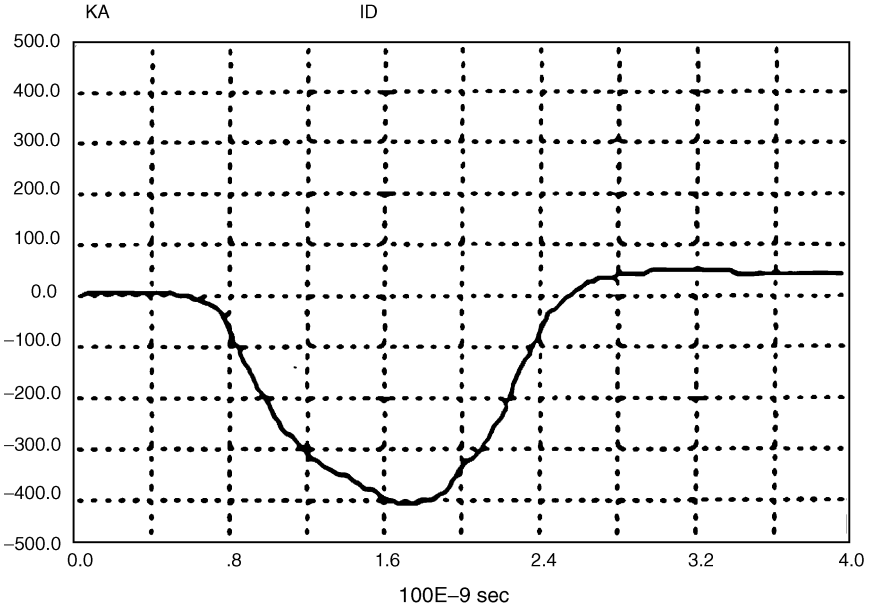
It is found that there is a close connection between the HPM generation and the diode pulse current waveform [10] in the experiment. For further discussion, diode voltage and current waveforms without microwave emission are given as shown in Fig. 6. We obtain that, after about 40 ns, plasma spreads over the whole cathode surface; after 100 ns, anode plasma begins to form; then space-charge bidirectional flow and beam pinching occur. For the case of HPM generation, an obvious difference will be easily marked by the feature of the diode current waveforms. Compared with the case of no HPM generation, the current here rises more slowly, which corresponds to the time that HPM emission starts.

There is an inflection point for most shots, as shown in Fig. 7. HPM generation terminates when the diode current reaches the self-pinching critical current of about 80 kA for the configuration studied. When the A–K gap is smaller than 1 cm, the diode current is increased to over 500 kA. Hence, the generated HPM has an evident pulse shortening effect accompanied with a multi-frequency feature resulting from the collapse and rebuilding of virtual cathode formation and beam reflection. Additionally, it can be drawn from the differential waveform of the current that

https://doi.org/10.1017/S0022377809007909 Published online by Cambridge University Press



(a)



(b)

Figure 6. Waveforms of diode (a) voltage and (b) current without microwave generation in the vircator studied.

the microwave pulse amplitude reaches its maximum value when di_D/dt on its minimum flat (shown in Fig. 8). The width of the HPM pulse corresponds to the time duration of the smaller absolute value of di_D/dt, and the falling time of the differential value corresponds to the rising of the HPM pulse.

https://doi.org/10.1017/S0022377809007909 Published online by Cambridge University Press

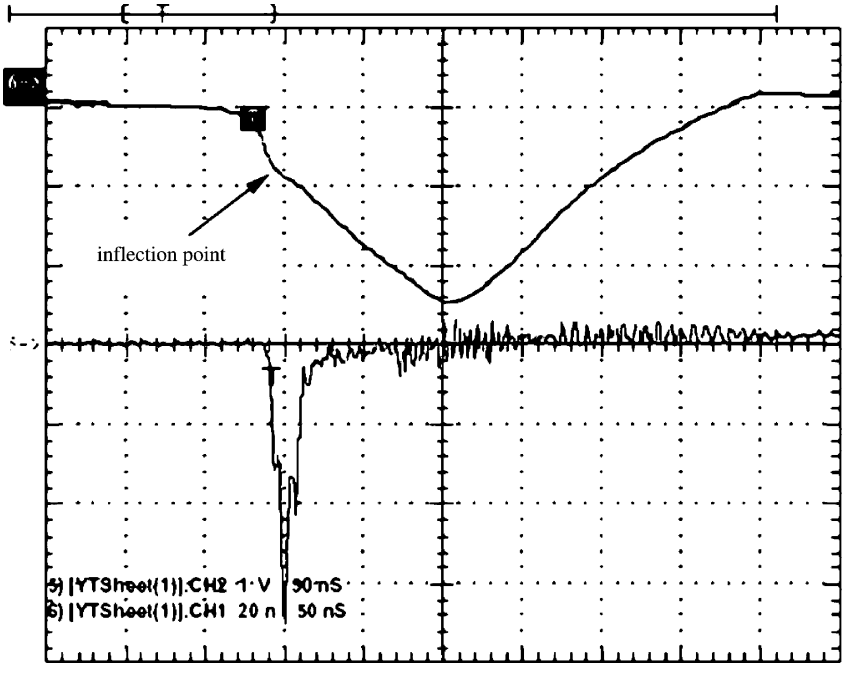


Figure 7. Waveforms of diode current (upper) with HPM generation (bottom) in the vircator.

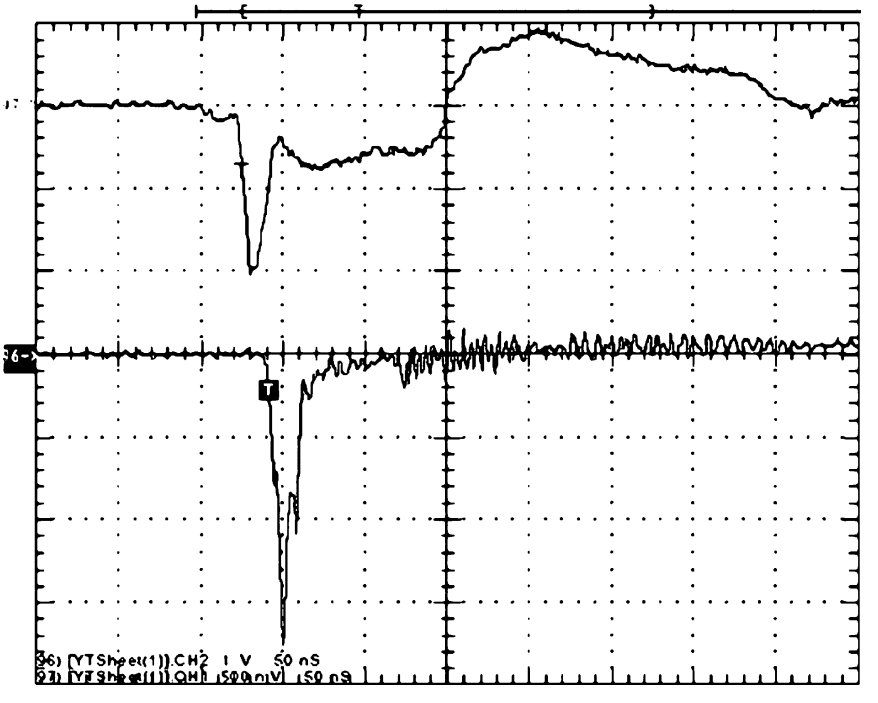


Figure 8. Differential waveforms in time of diode current (upper) with HPM (bottom) emission in the vircator.

https://doi.org/10.1017/S0022377809007909 Published online by Cambridge University Press

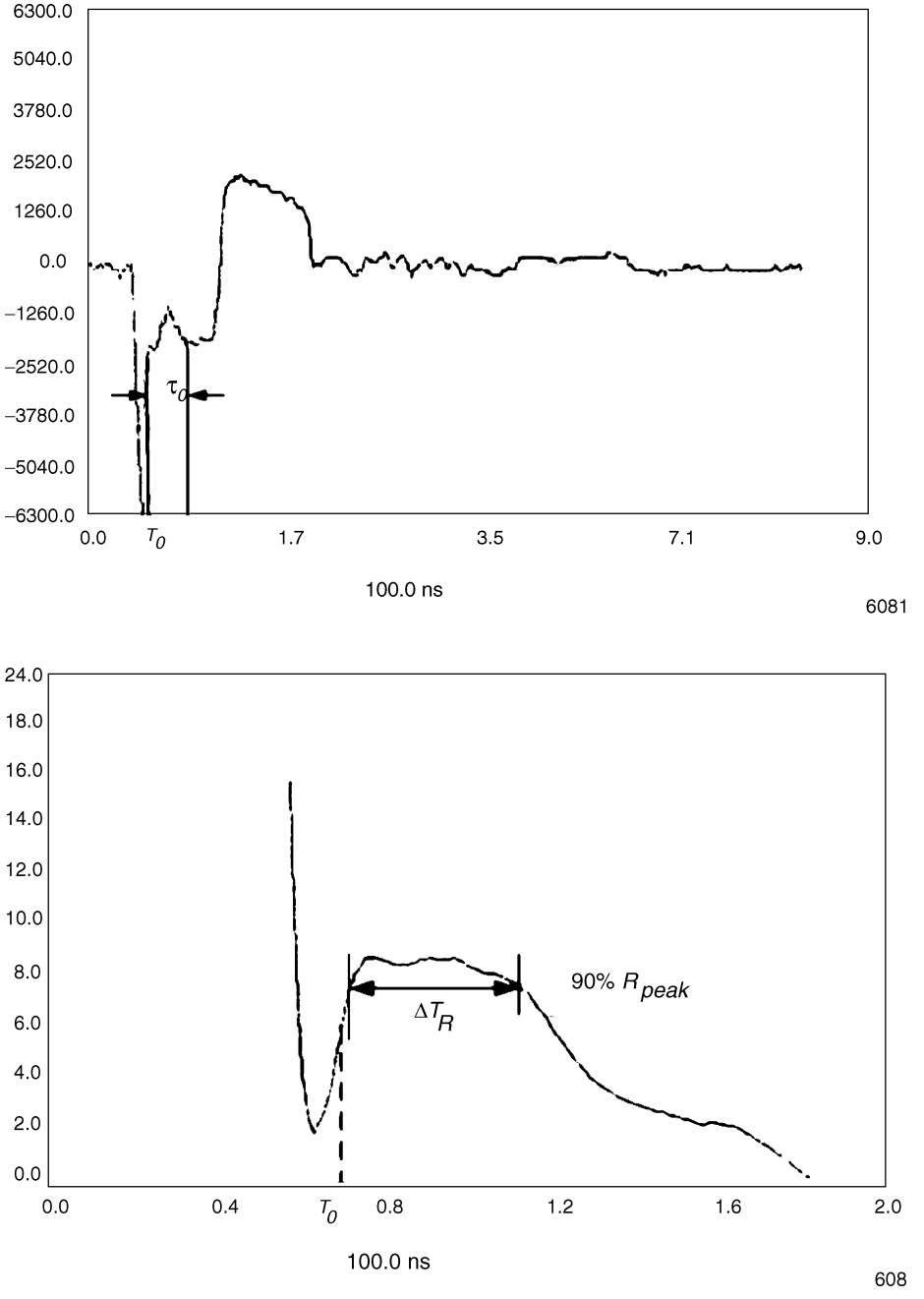


Figure 9. Differential waveforms of diode current and waveform of diode impedance with HPM generation.

Generally, it can be interpreted as follows: when the virtual cathode is formed and a HPM is generated, beam electrons are reflected into the diode region, resulting in a relatively stable modulation in the diode current. However, the plasma formed by beam electron bombardment on the anode results in a gradual decrease of the A–K gap, and the actual diode current will increase. When the diode current

https://doi.org/10.1017/S0022377809007909 Published online by Cambridge University Press

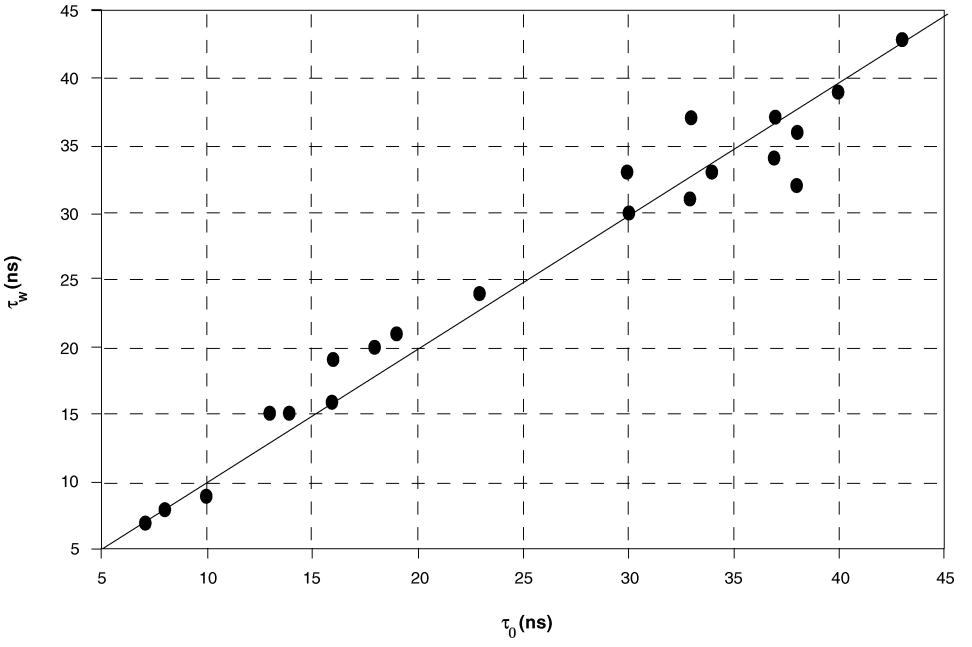


Figure 10. Comparison of HPM pulse width and τ_0.

approximately equals the self-pinching critical value, anode plasma formation will be accelerated. The interaction mechanism of the virtual cathode is broken by the high-density anode plasma, beam electrons will not be reflected any more, and, consequently, HPM emission terminates. After that, the increasing rate of the diode current recovers to the normal value.

It is found that the microwave pulse width could be estimated from the diode current waveform (or differential waveform of the current). Here we define T_0 as the starting time of HPM generation, τ_w is the HPM pulse width, and τ_0 is the time span of the differential current between the lagging edge of the first peak and the rising edge of the last peak, as shown in Fig. 9. The experimental results indicate that τ_w approximately equals τ_0 (see Fig. 10). T_R given in Fig. 9 is the time interval defined in the waveform of the diode impedance with the same characteristic. The comparison between T_R and τ_0 presents a remarkable consistency (see Fig. 11).

4. Conclusion

Experimental researches of a planar vircator system are reported and discussed. A novel spectrum diagnosis method—a circulating dispersion line—is proposed and employed in the experiment for properly evaluating the frequency components of a generated HPM pulse. An oil layer coated graphite cathode is introduced in the experiment to decrease the delay time of the explosive emission process and obtain a homogeneous electron beam emission for improving the HPM generation efficiency. HPM generation evidently depends on the diode current feature in which the rising rate of the diode current with HPM generation is obviously less than that of no HPM generation. For most cases, corresponding to the time that HPM generation starts, there is an inflection point in the diode current. Compared with that of

https://doi.org/10.1017/S0022377809007909 Published online by Cambridge University Press

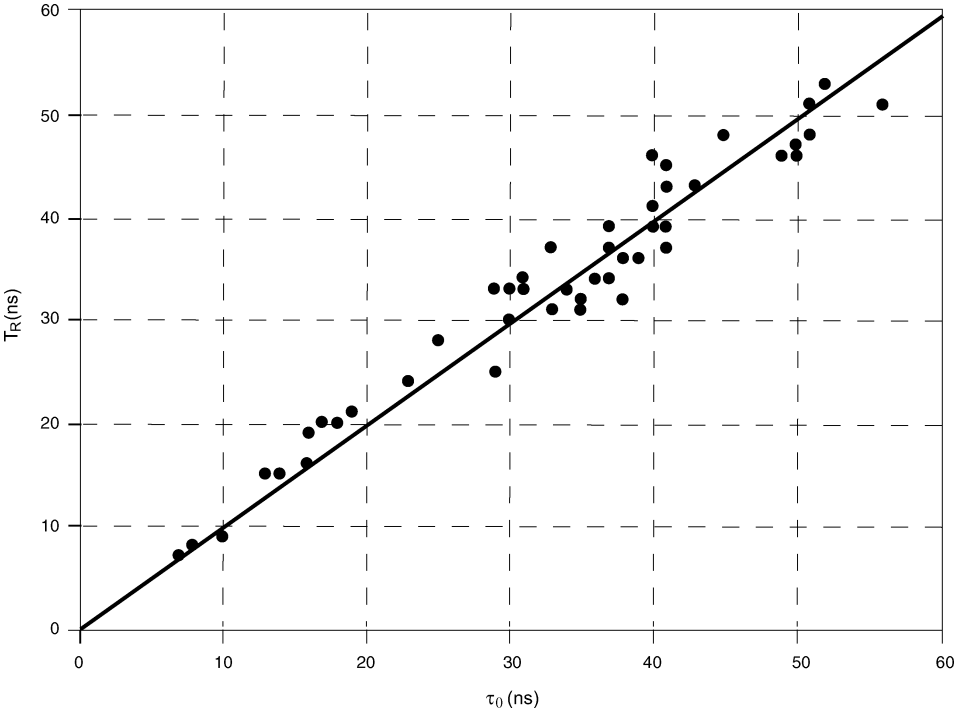


Figure 11. Relation of T_R and τ_0.

no HPM generation, the diode current increases more slowly after the inflection point. The microwave terminates when the diode current reaches the self-pinching critical current of the diode. Additionally, it can also be drawn from the differential waveform of the current that the microwave pulse reaches its maximum when di_D/dt is on its minimal flat. In other words, the microwave conversion efficiency and power will attain the highest flat when the diode current stays at a relatively constant value. During the HPM generation, the diode impedance is approximately constant, which corresponds to the HPM pulse width. A multi-frequency feature exists when the diode current exceeds five to ten times the space charge limiting current.

Acknowledgement

The authors would like to thank Dr Jianjun Huang, Mr Shuqing Ren, and Dr Junping Tang from the relativistic electron beam technology research group of the Pulsed Power Laboratory at the Northwest Institute of Nuclear Technology for their help with experiments.

References

[1] Guozhi, L. et al. 2006. Recent researches on coaxial vircator in NINT. In: *Proc. 1st Euro–Asia Pulse Power Conf., Chengdu*, pp. 538–544.

[2] Jiang, W., Woolverton, K., Diclens, J. and Kristiansen, M. 2001. Effect of electron-beam pulse length on microwave efficiency of coaxial vircator. In: *IEEE Proc. Pulsed Power & Plasma Science 2001 (PPPS 2001). Dig. Tech. Papers*, Vol. 2(6), pp. 1646–1648.

https://doi.org/10.1017/S0022377809007909 Published online by Cambridge University Press

[3] Kitsanov, S. A. et al. 2002. A vircator with electron beam premodulation based on high-current repetitively pulsed accelerator. *IEEE Trans. Plasma Sci.* **30**(1), 274–285.

[4] Jeon, W. et al. 2005. A diode design study of the virtual cathode oscillator with a ring-type reflector. *IEEE Trans. Plasma Sci.* **33**(6), 2011–2016.

[5] Liu, G. Z., Huang, W. H. and Wang, H. J. 1999. A ring of waveguide dispersive line for single short pulse microwave frequency analysis. *High Power Laser Part. Beams* **11**(2), 234–238 (in Chinese).

[6] Liu, G. Z. 2004. Physics of field-induced explosive emitting cathode. *Test Res.* **27**(3), 1–4.

[7] Liu, G. Z., Sun, J., Shao, H. and Yang, Z. F. 2005. Experimental study on effective emitting area of explosive emitting cathode. *High Power Laser Part. Beams* **17**(2), 249–252 (in Chinese).

[8] Changhua, C., Guozhi, L. and Wenhua, H. 2008. Advances in relativistic BWO operating repetitively. In: *Proc. BEAMS'2008, Xi'an, China*, July 2008.

[9] Woo, W.-Y. 1987. Two-dimensional features of virtual cathode and microwave emission. *Phys. Fluids* **30**(1), 239–244.

[10] Chen, X., Lindsay, P. A. and Zhang, J. 2000. Chaos and oscillations in a loaded plasma-filled diode. *IEEE Trans. Plasma Sci.* **28**(3), 462–471.

https://doi.org/10.1017/S0022377809007909 Published online by Cambridge University Press